Comparison of detailed reaction mechanisms for homogeneous ammonia combustion

L. Kawka[1], G. Juhász[1], M. Papp[1], T. Nagy[2], I. Gy. Zsély[1,*], T. Turányi[1]

[1] Institute of Chemistry, ELTE Eötvös Loránd University, Budapest, Hungary
[2] IMEC, RCNS, Eötvös Loránd Research Network, Budapest, Hungary

Abstract: Ammonia is a potential fuel for the storage of thermal energy. Experimental data were collected for homogeneous ammonia combustion: ignition delay times measured in shock tubes (247 data points in 28 datasets from 4 publications) and species concentration measurements from flow reactors (194/22/4).
The measurements cover wide ranges of temperature *T*, pressure *p*, equivalence ratio *φ* and dilution. The experimental data were encoded in ReSpecTh Kinetics Data Format version 2.2 XML files. The standard deviations of the experimental datasets used were determined based on the experimental errors reported in the publications and also on error estimations obtained using program MinimalSplineFit. Simulations were carried out with eight recently published mechanisms at the conditions of these experiments using the Optima++ framework code, and the FlameMaster and OpenSmoke++ solver packages. The performance of the mechanisms was compared using a sum-of-square error function to quantify the agreement between the simulations and the experimental data. Ignition delay times were well reproduced by five mechanisms, the best ones were Glarborg-2018 and Shrestha-2018. None of the mechanisms were able to reproduce well the profiles of NO, N_2O and NH_3 concentrations measured in flow reactors.

Keywords: ammonia combustion; detailed mechanisms; mechanism testing; shock tube ignition delay time measurements; flow reactor concentration profile measurements

1 Introduction

In recent years, there has been an increased interest in studying the combustion of NH_3. Sunshine and wind may provide large amount of energy, but the amount of electricity produced this way depends on weather. Electricity can be used for the electrolysis of water, and the energy content can be stored in the form of hydrogen gas. However, application of hydrogen as a fuel is problematic, since its diffusion velocity is high, and its efficient storage requires high pressure cylinders or very low (below -253 °C) temperature at 1 atm. Hydrogen can be stored very efficiently in the form of NH_3, since ammonia has 17.8% hydrogen content by mass.

Ammonia as a fuel has several advantageous properties [1,2]. It has a relatively high energy density (compared to liquid hydrogen) and its storage requirements are similar to those of propane, with similar boiling point and condensation pressure at room temperature. This means that the equipment designed for the storage and transport of propane is likely applicable also for ammonia. Also, there are several efficient methods for the direct production of ammonia from hydrogen and nitrogen gases, including the Haber-Bosch process. Production, storage, transport and utilization of ammonia is a more than 100-year old, well-established industry. However, combustion of ammonia also has multiple drawbacks, like high ignition temperature and low maximum burning velocity. Also, combustion of ammonia may produce large amount of NOx.

Practical utilization of ammonia in gas turbines and burners can be facilitated by the application of detailed reaction mechanisms. Intensive study of the chemical kinetics of ammonia combustion started just recently and a few mechanisms have been developed just for this purpose. However, since the oxidation pathways of NH_3 fuel are similar to the Thermal DeNOx and Zeldovich NO pathways in combustion NOx chemistry mechanisms, the latter mechanisms are applicable for the simulation of ammonia combustion. This is why experimental data for ammonia combustion have been compared by several authors with simulation results from mechanisms originally developed for NO formation in combustion systems. Testing results related to flames have been published in [1,3,4]. Stagnii *et al.* [3] compared measured and calculated ignition delay times at equivalence ratios $\varphi = 0.5, 1.0, 2.0$ in the initial temperature range of 1000–2500K.

In this paper our aim was to quantitatively describe the performance of recent detailed NOx chemistry reaction mechanisms on the description of ammonia oxidation at spatially homogeneous conditions based on shock tube and flow reactor measurements. Using least-squares error function value *E* allows us to investigate the performance of the mechanisms at the conditions of each set of measurements and also for each dataset separately. The changing performance of the description of the experimental data as a function of temperature and pressure will also be investigated. Analysis of this type has not been carried out on models of ammonia combustion.

2 Methodology

The agreement of the j-th measured and simulated values of the i-th dataset are characterized by the E_{ij} values:

$$E_{\mathrm{ij}} = \frac{Y_{ij}^{\mathrm{sim}} - Y_{ij}^{\mathrm{exp}}}{\sigma\left(Y_{i*}^{\mathrm{exp}}\right)} \quad (1)$$

where

$$Y_{ij} = \begin{cases} y_{ij} & \text{if } \sigma\left(y_{i*}^{\mathrm{exp}}\right) \approx \text{constant} \\ \ln y_{ij} & \text{if } \sigma\left(\ln y_{i*}^{\mathrm{exp}}\right) \approx \text{constant} \end{cases} \quad (2)$$

Here N is the number of datasets and N_i is the number of data points in the i-th dataset. Value y_{ij}^{exp} is the j-th measured data point, in the i-th dataset. The corresponding simulated (modelled) value is y_{ij}^{sim} obtained from a simulation using an appropriate detailed mechanism. If the error of measured values in data series i (i.e. y_{i*}^{exp}) can be characterized with an absolute error (i.e. their standard deviation is independent of the magnitude of y_{ij}), then we use them directly in the error function (i.e. $Y_{ij} = y_{ij}$). We used this option for a part of the concentration measurements. If the experimental results are described by relative errors (the scatter is proportional to the value of y_{ij}, thus it is constant on logarithmic scale), then we used the option $Y_{ij} = \ln y_{ij}$, which is characteristic for ignition delay time measurements. Measured concentrations may have either absolute or relative error.

The agreement of experimental and simulation results is investigated here using the following error functions:

$$E_{\mathrm{i}} = \frac{1}{N_i}\sum_{j=1}^{N} {E_{ij}}^2 = \frac{1}{N_i}\sum_{j=1}^{N}\left(\frac{Y_{ij}^{\mathrm{sim}} - Y_{ij}^{\mathrm{exp}}}{\sigma\left(Y_{i*}^{\mathrm{exp}}\right)}\right)^2 \quad (3)$$

$$E = \frac{1}{N}\sum_{i=1}^{N} E_i \quad (4)$$

Error function values E_i and E are expected to be near unity if the chemical kinetic model is accurate, and deviations of the measured and simulated results are caused by the scatter of the experimental data only. Note that due to the square in the definition of E, a twice higher deviation of the simulated and experimental values related to one mechanism in comparison to another leads to a four times higher value of E. This objective function has been used in our previous studies on the comparison of reaction mechanisms [5,6] and the estimation of rate parameters from experimental data [7–15].

In addition to the average error function E, the mean σ-normalized signed deviation D was used to characterize the behaviour of the mechanisms:

$$D_i = \frac{1}{N_i}\sum_{j=1}^{N} D_{ij} = \frac{1}{N_i}\sum_{j=1}^{N} \frac{Y_{ij}^{\mathrm{sim}} - Y_{ij}^{\mathrm{exp}}}{\sigma\left(Y_{i*}^{\mathrm{exp}}\right)} \quad (5)$$

$$D = \frac{1}{N}\sum_{i=1}^{N} D_i \quad (6)$$

where D_{ij} is the signed deviation for the j-th transformed data of dataset i. In contrast to E, the sign of difference $Y_{ij}^{\mathrm{sim}} - Y_{ij}^{\mathrm{exp}}$ is taken into account in the definition of D, thus positive and negative deviations can cancel each other out. Consequently, it measures systematic under- or overprediction, but its low value does not necessarily mean a good overall agreement.

Using rate-of-production analysis [16] the percentage contribution of each reaction step is investigated to the production and consumption rate of each species at several reaction times during the simulation. Revel et al. [17] suggested the investigation of the rate of the transfer of atoms from one species to another due to chemical reactions. This approach allows the creation of element flow graphs [16] which reveal the main reaction pathways.

3 The investigated mechanisms

Eight reaction mechanisms, published in the past eleven years for NOx combution chemistry, were selected for the comparison of simulation results with ammonia combustion experimental data. In the following, the mechanisms will be referred to by a short name containing the name of the first author

and the year of publication. The mechanisms are summarized in Table 1. This table also contains the number of species and reactions in the mechanism, and describes the carbon-free ammonia combustion experiments that were used for mechanism testing.

Mével *et al.* [18] measured ignition delay times of H_2–N_2O–Ar mixtures behind reflected shock waves. The experimental data were described with a new detailed reaction mechanism, which was also tested against delay time data from the literature for H_2–O_2–Ar, NH_3–Ar and H_2–N_2O–Ar mixtures.

Klippenstein et al. [19] investigated the role of NNH in NO formation and control. The work lead to the revision of the thermochemistry and reactions of NNH. Several NNH reactions were analysed using *ab initio* transition state theory based master-equation calculations incorporating high levels of electronic-structure theory and statistical rate theory.

The chemical kinetic model of Miller and Glarborg [20] was updated and presented as a new mechanism.

Abian *et al.* [21] investigated the formation of NO from N_2/O_2 mixtures in a flow reactor. Their mechanism is based on the previous mechanisms of Glarborg et al., with a reevaluation of the elementary reactions involved in thermal NO formation.

Zhang et al. [22] developed a detailed chemical kinetic mechanism to describe the pyrolysis and oxidation of the hydrogen/NOx and syngas/NOx systems. The thermodynamic data of nitrogenous compounds were updated based on the study of Bugler et al. [23]. The rate parameters were selected through a comparison of the data available in the literature and the adoption of the latest available published rate constant data. The proposed mechanism was validated against a large number of literature experimental data.

Glarborg et al. [24] wrote a very comprehensive review on the nitrogen chemistry in combustion systems. They updated the thermochemistry of the nitrogen compounds using the Active Thermochemical Tables (ATcT) approach. Rate parameters for the nitrogen species were surveyed. The results of the review were also summarized in a new recommended detailed reaction mechanism, which describes the reactions of nitrogen oxides during natural gas combustion.

Shrestha et al. [25] created a detailed kinetic mechanism to describe the oxidation of ammonia. The mechanism was tested on literature data related to freely propagating and burner-stabilized premixed

flames, and also on shock-tube, jet-stirred reactor, and plug-flow reactor experiments. The work mainly focused on pure ammonia and ammonia–hydrogen fuel blends.

Song et al. [26] investigated the sensitizing effects of NO_2 and NO on methane low-temperature oxidation in a jet stirred reactor. The experimental results were interpreted with the latest version of the POLIMI mechanism.

Kovács et al. [15] published an optimized reaction mechanism for the N/H/O system which was based on the Glarborg-2018 [24] and ELTE syngas [8] mechanisms. Several rate parameters of this mechanism were tuned by fitting to indirect data, obtained from experiments of hydrogen–oxygen combustion perturbed with nitrogen oxides.

Looking at the list of mechanisms, it is clear that the Shrestha-2018 mechanism is the only one that was directly created for the description of NH_3 combustion. As Table 1 shows, most of the investigated mechanisms were tested by the original authors on ammonia combustion or pyrolysis data. We consider that it is an important knowledge if mechanisms containing nitrogen chemistry in combustion systems are able to describe ammonia combustion. This also means that a poor performance in this test does not imply that the mechanism is not well applicable at the conditions it was originally developed for.

Table 1. The reaction mechanisms used in the comparison. The mechanism names are abbreviated with the name of the first author and the year of the corresponding publication. The number of species and reactions refer to the H/N/O submechanism of the original reaction mechanism. Experiemental types: ST-IDT ignition delay measurements in shock tube, FLOW-C concentration measurements in flow reactor, FLAME-C concentration measurements in flames, VL burning velocity measurement

Mechanism	Ref.	No. of species	No. of reactions	Experimental conditions of mechanism testing						
				system	expt. type	*T* range / K	*p* range / bar	phi range	diluents	dilution range
Mével-2009	[18]	32	215	NH_3 pyrolisis	ST-IDT	2300-3300	1	1	Ar	0.992-0.999
Klippenstein-2011	[19]	37	219	NH_3/O_2	ST-IDT	2160	5.1	1.33	Ar	0.984
				NH_3/O_2 or $NH_3/NO/H_2$ or $NH_3/NO/H_2O$	FLOW-C	920-1335	1	<0.001 -0.04	N_2	0.445-0.959
Abian-2015	[21]	37	219	not tested						

Zhang-2017	[22]	44	198	NH_3/O_2	ST-IDT	1560-2455	1.4-30	0.5-2	Ar	0.98-0.99
Glarborg-2018	[24]	35	207	NH_3/O_2	ST-IDT	1900-2500	1.4	0.5-2	Ar	0.99
				$NH_3/NO/O_2$	FLOW-C	930-1380	1	0.002	N_2	0.577-0.603
				NH_3/O_2	FLAME-C	room	0.046	0.71	Ar	0.01
Shrestha-2018	[25]	34	278	NH_3/O_2	ST-IDT	1560-2455	1.4-30	0.5-2	Ar	0.98-0.99
				$NH_3/H_2/N_2O$	FLOW-C	995	3	1.02	N_2	0.982
				NH_3/O_2/Ar (/NO)(/H_2)	FLAME-C	298	0.046-0.072	0.12-1.91	Ar	
				NH_3/air(/H_2)	VL	293-298	1-5	0.1-4	N_2	
Song-2019	[26]	29	149	not tested						
Kovács-2020	[15]	34	214	not tested						

4 Collection of experimental data

A large set of experimental data was collected related to ammonia combustion. The data belong to two types of measurements, ignition delay times measured in shock tubes and concentrations measured in flow reactors. Our intention was to locate all ammonia combustion measurements in these categories.Collection of ignition delays in rapid compression machines (RCMs), jet-stirred reactors (JSRs), burning velocity measurements and species profile measurements in burner stabilized flames are in progress and such measurements will not be considered in this paper.

All collected data were encoded in Respecth Kinetics Data format files, according to the latest (version 2.2) specification [27]. The RKD format is an XML data format for the storage of indirect combustion measurements (like ignition delay times and laminar burning velocity measurements) and rate coefficient determinations by direct gas kinetics experiments and theoretical calculations. The RKD format is a modified and extended version of the PrIMe Kinetics Data Format [28]. The RKD files contain all information required for the simulation of the experiments and the calculation of properties observed or derived from experiments (*e.g.* the ignition delay time as defined in the corresponding experimental publication). All data files discussed in this article are available from the ReSpecTh Information Site [27]. The RKD Format xml files can be downloaded from the ReSpecTh site (http://respecth.chem.elte.hu/respecth/reac/dofile.p

hp?file=newZip/NH3_indirect.zip).
An overview of the ignition delay time measurements [29–32] and flow reactor [33–36] used here are given in Table 2. Supplementary Tables 1 and 2 provide more detailed information about each dataset. Another paper on the measurement of shock tube ignition delays of NH_3/O_2 mixtures was also found, but the authors Dove and Wing [37] carried out their measurements in krypton. These data were not used here since none of the reaction mechanisms used contain Kr as buffer gas.

Table 2. Brief summary of the collected experiments

Publication	No. of datasets	No. of data points	Composition	Diluent	p / atm	T / K	phi range
Shock tube ignition delay times							
Fujii et al. [29]	4	46	$NH_3/O_2(/H_2)$	Ar	5–8.55	1359–2098	0.750–0.825
Drummond [30]	6	67	NH_3/O_2	Ar	0.25–35.8	1542–2586	0.375–0.750
Mathieu and Petersen [31]	12	104	NH_3/O_2	Ar	1.29–30.4	1564–2489	0.500–2.000
Shu et al. [32]	6	30	NH_3/O_2	N_2	15.9–41.6	1181–1581	0.501–1.994
Species concentration in flow reactor							
Hulgaard and Dam-Johansen [33]	5	50	NH_3/O_2 $(/H_2O)$	N_2	1.04	938–1373	0.022–0.024
Wargadalam et al. [34]	4	36	NH_3/O_2 $(/H_2)$	N_2	1.0	873–1274	0.002–0.003
Song et al. [35]	10	63	NH_3/O_2	N_2	29.6, 98.7	450–925	0.013–0.623
Caton et al. [36]	3	45	NH_3/O_2	N_2	1.0	798–1200	0.005

5 Simulation of experiments

Optima++ was used as a framework code to perform simulations for each mechanism on all data sets. Optima++ can be downloaded from the ReSpecTh information site [27]. Optima++ may use either the FlameMaster [38] or the OpenSmoke++ [39,40] simulation packages. In the case of using any of the two simulation packages, Optima++ selects the type of simulation, like adiabatic constant volume 0D simulation for simulating an appropriate shock tube experiment, sets up the input files from the RKD-format datafiles, performs the simulations and collects the results without human interaction. The

complete investigation of a mechanism against even several thousand experimental data points can be carried out in a single run. To check the possible dependence of the results on the choice of the simulation package, all calculations were carried out with both packages. We found that the results were practically identical, a correlation coefficient more than 0.99 was found for the pointwise results.
Ignition delay times were extracted from the simulated pressure or concentration profiles, and interpreted as described in the respective publications, e.g. based on the maximum slope of the pressure profile or baseline intercept from d[OH*]/dt, where OH* denotes electronically excited OH radical. Three reaction mechanisms (Klippenstein-2011 [19], Abian-2015 [21] and Song-2019 [26]) did not contain excited OH chemistry. The relevant reactions were added to these mechanisms from AramcoMech2 [41].

6 Estimation of the experimental uncertainty

In equations 1, 3 and 5, division by the estimated standard deviation of the experimental data means that the results of the different experiments are represented on the same scale, relative to their own uncertainty. A good estimation of the standard deviation is crucial, but unfortunately these are missing from even the most recent publications. Besides the experimentally reported uncertainties, the estimated standard deviations of the datasets were also considered. If the standard deviation estimated by computer code MinimalSplineFit [42] from the experimental noise of the data points for each dataset was higher than the reported standard deviation the estimated value was used in the calculations.
Ignition delay time errors were reported in the paper of Mathieu et al. [31] (10% for pressures below 16 bar and 20% for higher pressures) and Shu et al. [32] (20%), therefore we used these uncertainties for these measurements. Concentration measurement errors were reported in the paper of Hulgaard et al. [33] (2 ppm for N_2O, 3 ppm for NH_3), Wargadalam et al. [34] (maximum 10% for the measurements of N_2O, NO, CO, CH_4, CO_2, HCN, and NH_3), and Song et al. [35] (2-6% for NH_3/NO/NO_2). Assuming constant relative error when very low concentrations are measured is impractical, as it would artificially overweight the contribution of

those points to the error functions. Taking also into account papers of Alzueta et al. [43,44], 10% relative error, but at least 2 ppm for NO and N_2O, and 10 ppm for NH_3 was used in this work. All 1σ standard deviation values used in this work are given in Supplementary Tables 3 to 6.
Although we considered the experimental uncertainty given in the original publications and the uncertainty used was sometimes increased from the reported one if the data had a large scatter, it is clear that large systematic error may also be present. This is probably less significant for the shock tube measurements, but in the flow reactor experiments species may adsorb to the wall and the wall may have catalytic effect. Significant difference between the measured and simulated data may come from missing important reactions, wrong rate parameters of important reactions or large systematic error of the measurements.

7 Results and discussion

The performance of ammonia combustion mechanisms were analysed using the *E* and *D* functions. As it has been discussed in Section 2, *E*=1 means that the experimental and simulation data are in good agreement and the only reason of discrepancy is the statistical error of the experiments. Value *E* lower than 4, 9, 16, etc. means that the simulations reproduce the measurement data on average within their 2σ, 3σ, 4σ standard deviation, respectively. According to our previous experience [5,6], *E* values below 4 and 9 can be considered as a good and an acceptable, respectively, reproduction of the measurements with simulations. High *E* value may indicate that the mechanism is not appropriate for the reproduction of a given dataset, but is also might indicate a large systematic error of the measurement. However, if at least one of the mechanisms provide a low *E* value for a dataset, while some other mechanisms give high *E* values, then probably the systematic error is not significant.

7.1 Comparison of measured and simulated

ignition delay times

The squared mean deviation function (E) revealed that the ignition delay can be reproduced the best by the Glarborg-2018, Shrestha-2018 and Kovács-2020 mechanisms, while the Klippenstein-2011, Abian-2015 and Zhang-2017 mechanisms produced only slightly worse results. The Mevel-2009 mechanism was not able to reproduce the ignition delays with acceptable accuracy except for the measurements of Shu et al. [32], and the Song-2019 mechanism failed to describe the experiments of Fujii et al. [29] and Mathieu et al. [31].

Table 3. Averaged E values for the ignition delay time experiments of each publication. The summation in Eq. 3 ran on all datasets of each publications, separately.

	Mevel-2009 [18]	Klippenstein-2011 [19]	Abian-2015 [21]	Zhang-2017 [22]	Glarborg-2018 [24]	Shrestha-2018 [25]	Song-2019 [26]	Kovács-2020 [15]
Fujii et al. [29]	57.8	7.9	7.9	6.9	11.4	7.0	35.3	12.1
Drummond [30]	136.1	12.6	12.6	9.6	5.3	10.3	112.5	5.2
Mathieu and Petersen [31]	153.5	10.2	9.9	8.4	4.2	8.7	93.6	4.6
Shu et al. [32]	19.3	15.6	16.8	37.0	13.9	4.9	17.6	14.6
Average by datasets	101.9	11.2	11.3	14.3	7.4	7.7	69.7	7.8

The dependence of the E_{ij} values on the initial conditions was investigated and some interesting patterns were found. The two weakly performing mechanisms reproduced the ignition delay times much better for low and high temperatures than for the medium ones (Figure 1 shows this behaviour for the Song-2019 mechanism). The better performing mechanisms show similar dependence, but much less obviously.

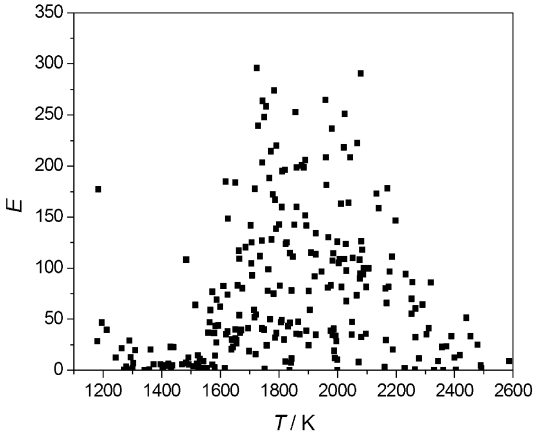

Fig. 1. Plot of the E_{ij} values versus temperature calculated by the Song-2019 mechanism.

The mechanisms typically reproduced the higher pressure measurements (20 atm and above) better than the lower ones. For example the Shrestha-2018 mechanism did not reproduce well the results of several low-pressure experiments (Fig. 2.).

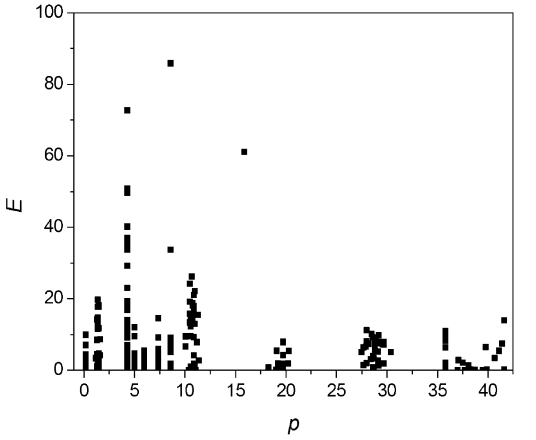

Fig. 2. Plot of the E_{ij} values versus pressure calculated by the Shrestha-2018 mechanism.

The picture is a bit different if we consider the signed deviation function *D*. As it has been discussed in Section 2, low *D* value does not mean that there is a good agreement between the measured and simulated data, but high positive and high negative value indicate the simulations systematically overpredict and underpredict, respectively, the experimental values.
Table 4 shows that the experiments of Fujii et al. [29] and Shu et al. [32] are typically overpredicted, but those of Drummond [30] and Mathieu and Petersen [31] are underpredicted. The Mevel-2009 mechanism

underpredicts almost all datasets (except one, see Supplementary Tables 3 and 4). The Glarborg-2018 mechanism seems to reproduce well the experiments of Drummond *et al.* and Mathieu *et al.*, but behind the good averages both over- and underpredictions appear.

Table 4. Averaged *D* values for the ignition delay time experiments of each publication.The summation in Eq. 6 ran on all datasets of each publications, separately.

	Mevel-2009 [18]	Klippenstein-2011 [19]	Abian-2015 [21]	Zhang-2017 [22]	Glarborg-2018 [24]	Shrestha-2018 [25]	Song-2019 [26]	Kovács-2020 [15]
Fujii et al. [29]	–4.4	0.5	0.5	2.0	2.5	0.0	–2.5	2.3
Drummond [30]	–5.5	–1.8	–1.8	–1.4	–0.1	–1.5	–5.3	0.1
Mathieu and Petersen [31]	–6.1	–2.3	–2.2	–2.1	0.1	–1.9	–5.5	–0.1
Shu et al. [32]	–1.6	5.7	6.1	13.3	5.0	1.3	3.9	5.3
Average by datasets	–4.5	0.0	0.1	2.0	1.5	–0.8	–2.8	1.4

Figure 3 shows how the signed deviation values D_{ij} depend on pressure. The ignition delay times measured around 10–11.5 atm and 27–30 atm are underpredicted by all reaction mechanisms.

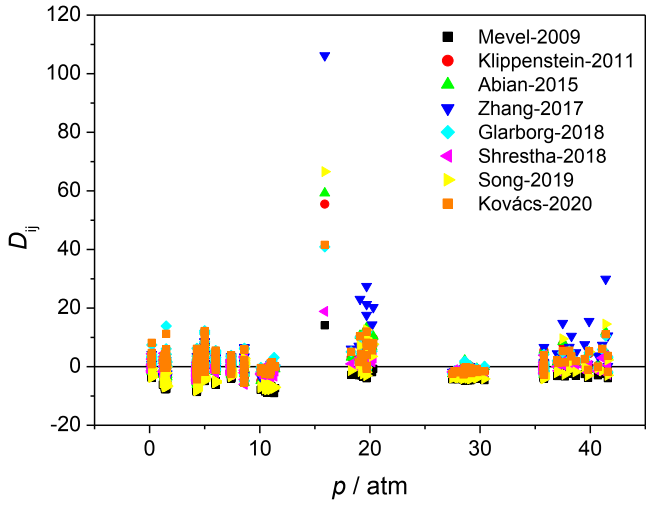

Fig. 3. Plot of the D_{ij} values versus pressure calculated by all reaction mechanisms used considering the ignition delay time experiments.

Typical temperature dependences of the signed deviation value D_{ij} are presented in Figure 4. For the Mevel-2009 and Song-2019 mechanisms a U-shaped dependence can be found with strong underprediction, whereas for the Glarborg-2018 mechanisms, and especially for the Shrestha-2018

mechanism a much more balanced pattern can be seen.

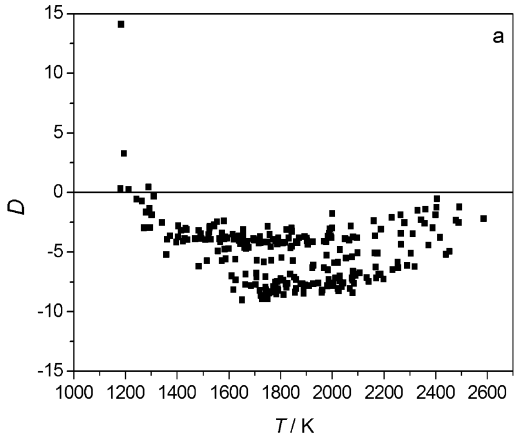

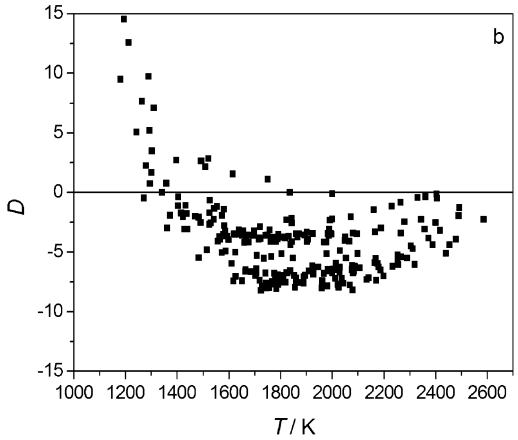

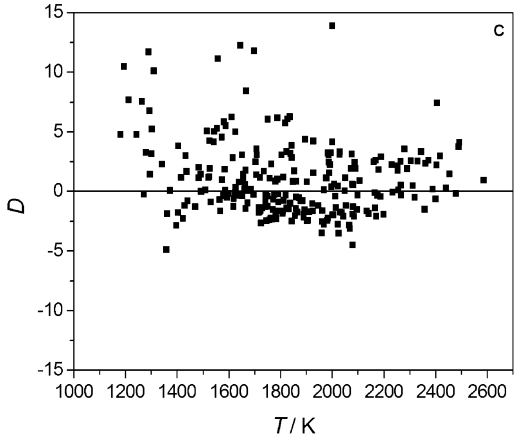

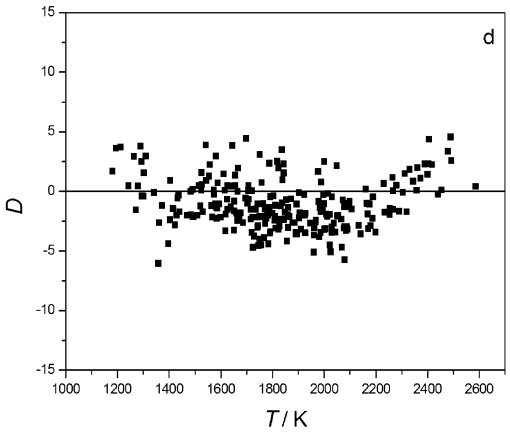

Fig. 4. Plot of the D_{ij} values versus initial temperature calculated by mechanisms Mevel-2009 (a), Song-2019 (b), Glarborg-2018 (c) and Shrestha-2018 (d).

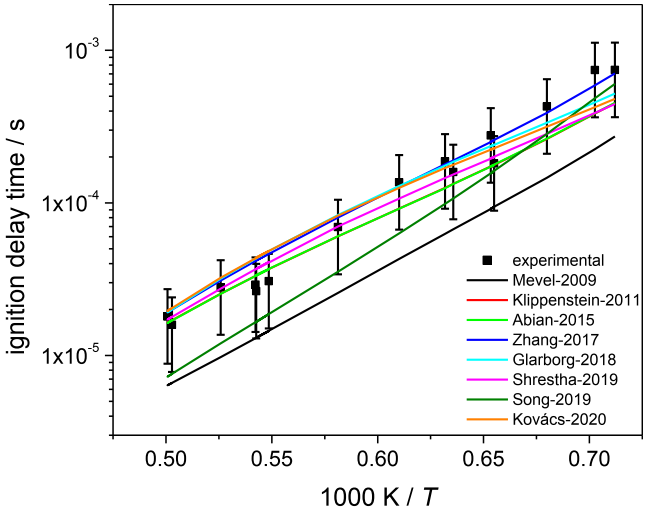

Fig. 5. Ignition delay time measurements of Fujii et al. [29] (pressure 7.4 atm, inlet mole fractions $x(NH_3)$=0.05, $x(H_2)$=0.003, $x(O_2)$=0.05, x(Ar)=0.897). The indicated error bars belong to 3σ. The simulation results are given with solid lines for each investigated mechanism.

Figure 5 presents a log ignition delay time – reciprocal temperature graph for the reproduction of one of the experimental series of Fujii et al. [29]. This graph shows that the *E* and *D* values given in Tables 3 and 4, respectively, really well characterize the level of reproduction of the experimental data and the systematic under and overpredictions.

7.2 Exploration of the reasons of deviations in the ignition delay time predictions

The deviations of the performances of the mechanisms were investigated by rate-of-production and element flow analyses.
The key reaction steps of the ignition of ammonia are the hydrogen removal reactions from NH_3 (see also Fig 26 in Glarborg et al. [24]), therefore the consumption of NH_3 is in the center of interest. Rate-of-production analysis was carried out at one of the experimental conditions of Fujii et al. [29]. In this experiment (x1019901p7) ammonia is ignited by oxygen diluted in argon at slightly lean condition, and at medium temperature and pressure. Two mechanisms were selected which performed very differently at the conditions of this experiment: Shrestha-2018 was a good performing (E = 2.79) and Song-2019 was an ill-performing (E = 112) mechanism. Both mechanisms predict faster ignition delay times than the experimental one. The rate-of-production analysis revealed that the ammonia consumption is much faster during the induction period for the Song-2019 mechanism by almost one magnitude. Table 5 shows the main production and consumption reactions in an early time point (near 10 μs) of the induction period. The exact times (t = 10.4 μs and 10.7 μs for the Shrestha-2018 and Song-2019 mechanisms, respectively, were determined in such a way that the calculated temperature is identical T = 1735 K.

Table 5. Rate of formation and consumption of NH_3 for the experiment of Fujii et al. (x1019901p7) [29] calculated by mechanisms Shrestha-2018 [25] (Table a), t = 10.4 μs) and Song-2019 [26] (Table b), t = 10.7 μs). Reactions having more than 10% contribution are shown.

a)

Shrestha-2018 at t = 10.4 μs	rate of formation (–) / production (+) / (kmol/m^3/s)	contribution in formation (–) / production (+)
total NH_3 formation rate	$5.23 \cdot 10^{-5}$	
$2\ NH_2 = NH + NH_3$	$4.86 \cdot 10^{-5}$	33.9%
$N_2H_3 + NH_2 = H_2NN + NH_3$	$4.50 \cdot 10^{-5}$	31.4%
$HO_2 + NH_2 = NH_3 + O_2$	$3.23 \cdot 10^{-5}$	22.6%
$NH_3 + O = NH_2 + OH$	$-5.08 \cdot 10^{-3}$	–15.9%
$HO_2 + NH_2 = NH_3 + O_2$	$-9.18 \cdot 10^{-3}$	–28.8%
$NH_3 + OH = H_2O + NH_2$	$-1.02 \cdot 10^{-2}$	–32.1%
total NH_3 consumption rate	$-3.18 \cdot 10^{-2}$	

b)

Song-2019 at t = 10.7 μs	rate of formation (–) / production (+) / (kmol/m^3/s)	contribution in formation (–) / production (+)
total NH_3 formation rate	$2.17 \cdot 10^{-3}$	
2 NH_2 = NH + NH_3	$1.58 \cdot 10^{-3}$	62.6%
HNO + NH_2 = NH_3 + NO	$7.32 \cdot 10^{-4}$	29.1%
H + NH_3 => H_2 + NH_2	$-2.34 \cdot 10^{-2}$	–11.6%
NH_3 + O => NH_2 + OH	$-6.22 \cdot 10^{-2}$	–30.9%
NH_3 + OH => H_2O + NH_2	$-9.33 \cdot 10^{-2}$	–46.4%
total NH_3 consumption rate	$-2.01 \cdot 10^{-1}$	

Two reactions are responsible for 75% of the ammonia consumption in the Song-2019 mechanism: NH_3+O=>NH_2+OH and NH_3+OH=>H_2O+NH_2. The reason of the large difference in the consumption rate can be seen in the Arrhenius plots of the reactions (Fig. 6). The rate coefficient of reaction NH_3+O=>NH_2+OH is somewhat faster in the higher temperature range in the Song-2019 mechanism (taken from the work of Corchado and Espinosa-Garcia [45]), than that of the Shrestha-2018 mechanism (Arrhenius expression of Baulch et al. [46]). The difference in the rate coefficients for reaction NH_3+OH=>H_2O+NH_2 is much larger, it is almost one magnitude larger in the Song-2019 mechanism. For this reaction in the Shrestha-2018 mechanism the Arrhenius parameters are from the PhD Thesis of P. Klaus [47], in the Song-2019 mechanism the values are taken from the work of Sutherland et al. [48].

(a)

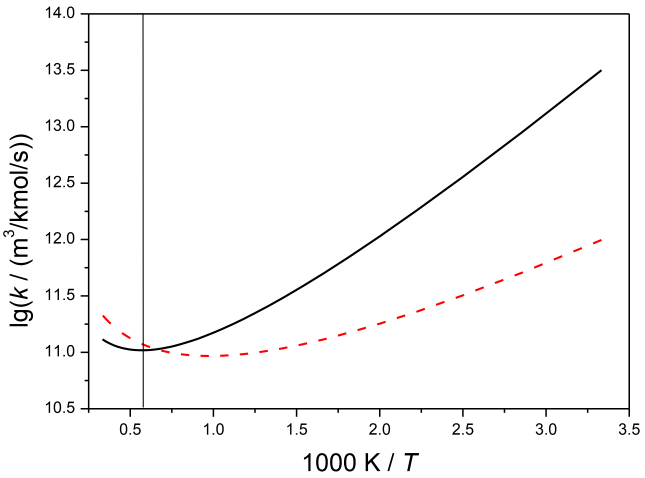

(b)

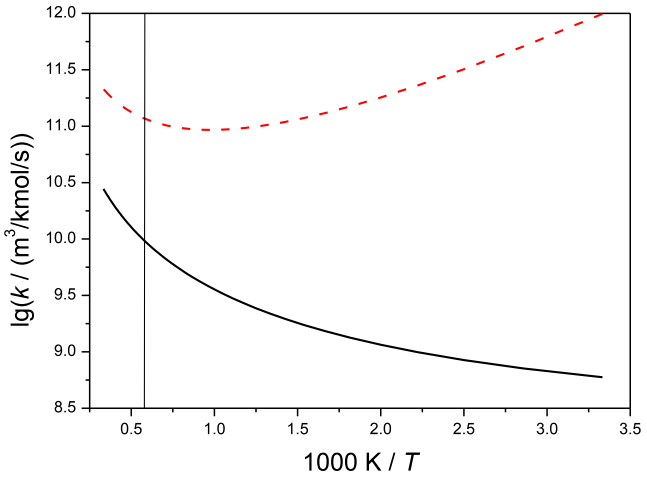

Fig. 6. Arrhenius plots for reactions NH_3+O=>NH_2+OH (a) and NH_3+OH=>H_2O+NH_2 (b). Lines represent the rate coefficient values for mechanisms Shrestha-2018 [25] (solid black) and Song-2019 [26] (dashed red). The vertical line denotes the temperature of the rate-of-production analysis.

Analysis of element fluxes was also applied at the same condition. Program Optima++ generated the fluxes for elements H, O, and N, and these were visualized by program Fluxviewer++. Since we mainly interest in the nitrogen-containing species, only the N-fluxes are shown. Figure 7 shows the fluxes at a later time point (40 μs), where the reaction network is much more evolved. At this time the important pathways (via NH and NO) are not fully developed according to the Shrestha-2018 mechanism (Figure 7 (a)), while these are fully developed according to the Song-2019 mechanism (see Figure 7 (b)). The graphs shows that species N_2H_2 and H_2NO are important intermediates between NH_2 and NNH, NH_2 and HNO, respectively.

(a)

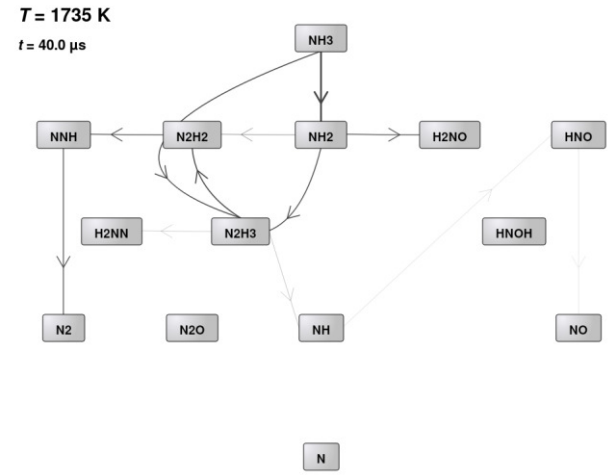

(b)

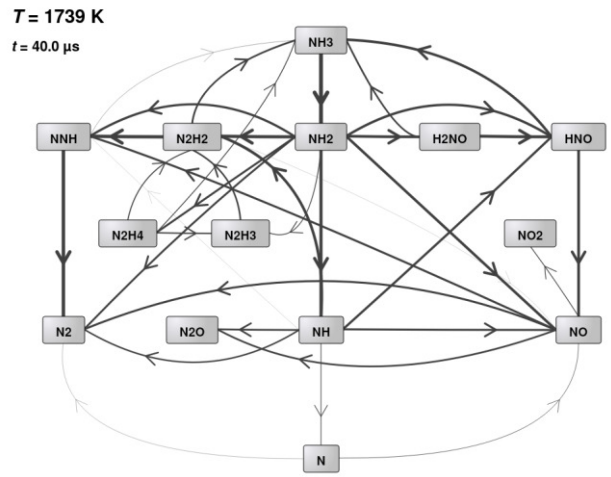

Fig. 7. N-atom flux graphs at time 40 μs during the induction period of the experiment of Fujii et al. (x1019901p7) [29], according to (a) Shrestha2018 mechanisms [25], (b) Song2019 mechanism [26].

Figure 8 shows similar graphs just berore the ignition, belonging to temperature *T*=2285 K. Unlike at the beginning of the induction period, near the ignition time the figures belonging to the two mechanisms are qualitatively similar to each other. Program Fluxvier++ can prepare animated gifs from a series of pictures. Two animations related to this analysis can be found among the Supplementary files.

(a)

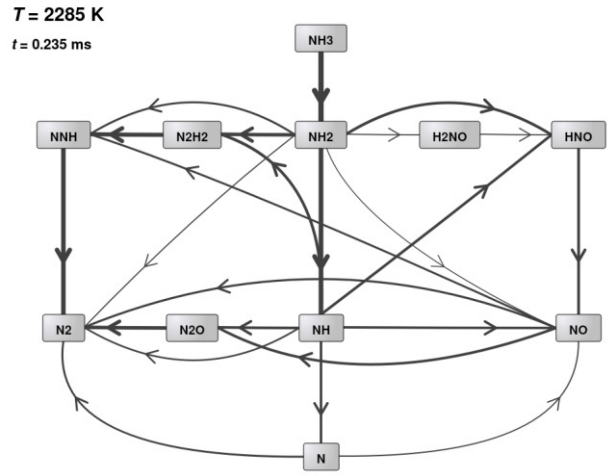

(b)

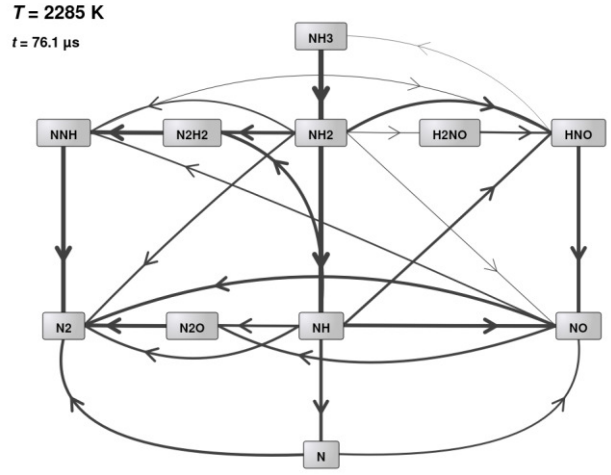

Fig. 8. N-atom flux graphs just before the ignition in the experiment of Fujii et al. (x1019901p7) [29]. (a) Shrestha-2018 mechanisms [25], (b) Song-2019 mechanism [26].

7.3 Comparison of measured and simulated concentrations of flow reactor experiments

In the flow reactor experiments, concentrations of four species (NO, N_2O, NH_3 and O_2) were measured (NH_3 in all four papers, NO in the works of Hulgaard and Dam-Johansen [33], Wargadalam et al. [34] and Caton et al. [36], N_2O in Hulgaard and Dam-Johansen [33], Song et al. [35] and Caton et al. [36]; O_2 was measured only by Song et al. [35]). The change of O_2 concentrations in the expertiments was very small and it was well reproduced by the mechanisms. For the nitrogen containing species, there were 7 data points for which the error function value was above

5000 using any reaction mechanisms. Checking the simulations related to these data points (experiments of Song et al. [35], all 4 data points in x30199015.xml (Fig. 7 black stars in the original publication), and 3 data points in x30199016.xml (Fig. 7 black squares having higher temperature than 850 K in the original publication)), no technical error was found, therefore these data points as possibly problematic ones were filtered out from the averaging. The results show that the best mechanisms for the description of the concentration measurements in flow reactor experiments are Zhang-2017 and Shrestha-2018, however, their *E* values are still far larger than being acceptable. The average deviation is larger than 7σ. The Shrestha-2018 mechanism is good on average, but is not the best one for any of the species. The best mechanisms were Song-2019 for the NO measurements, Kovács-2020 for the N_2O measurements and Zhang-2017 for the NH_3 experiments. For NO, only the Song-2019 mechanism gave acceptable simulation results, but this mechanism failed for N_2O and NH_3. As a conclusion, there is no single reaction mechanism which can reproduce all flow reactor data. Glarborg et al. [24] noted that the surface reactions have a high impact on ammonia oxidation even using quartz surfaces. Therefore, flow and batch reactor experiments are not recommended for model validation. Our findings are in good agreement with this statement.

Table 6. Average *E* values for the concentration measurements in flow reactor experiments.

	No. of data points	Mevel-2009 [18]	Klippenstein-2011 [19]	Abian-2015 [21]	Zhang-2017 [22]	Glarborg-2018 [24]	Shrestha-2018 [25]	Song-2019 [26]	Kovács-2020 [15]
NO	56	240.2	222.3	219.5	142.4	442.2	196.7	18.5	419.5
N_2O	55	65.4	76.1	78.9	40.9	25.6	47.9	268.6	23.43
NH_3	70	388.7	97.4	83.7	22.6	128.7	30.1	45.5	106.9
O_2	13	0.13	0.13	0.13	0.13	0.13	0.13	0.13	0.13
Average by datasets		231.5	111.1	105.7	61.0	160.1	70.1	96.1	145.5

Table 7. Average *D* values for the concentration measurements in flow reactor experiments.

	No. of data points	Mevel -2009 [18]	Klippenstein-2011 [19]	Abian -2015 [21]	Zhang -2017 [22]	Glarborg-2018 [24]	Shrestha-2018 [25]	Song-2019 [26]	Kovács -2020 [15]
NO	56	14.9	4.7	4.5	1.5	2.4	3.2	2.1	2.0
N_2O	55	1.5	–0.8	–0.9	–1.0	0.8	–0.5	–1.7	0.6
NH_3	70	–1.6	0.1	0.1	0.3	0.9	0.1	0.5	0.8
O_2	13	0.2	0.2	0.2	0.2	0.2	0.2	0.2	0.2
Average by datasets		3.1	0.9	0.9	0.2	1.1	0.6	0.3	1.0

The average signed deviations for NO are the largest, but it doesn't mean that for NH_3 and N_2O most of the datapoints are well simulated. The very high *D* value related to the Mevel-2009 mechanism for the NO is supported by the results presented in Figure 9, which shows overprediction in almost all cases. The other mechanisms over- and underpredict the measured NO concentrations in a more balanced way.

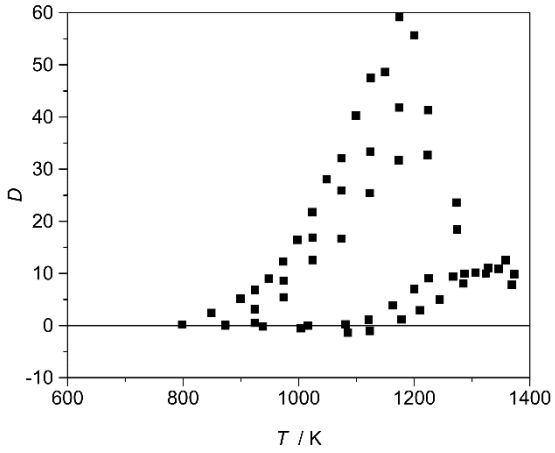

Fig. 9. Plot of the D_{ij} values versus temperature calculated by mechanism Mevel-2009 for the NO measurements in flow reactors.

The prediction of the N_2O concentration exhibits typical patterns as shown in Figure 10. Experiments of Caton et al. [36] are overpredicted by all mechanisms except Song-2019. Experiments of Song et al. [35] are underpredicted by all mechanisms except Glarborg-2018 and Kovács-2020. Experiments of Hulgaard and Dam-Johansen are quite well reproduced, except for a few of the highest temperature measurement points and by the Song-2019 mechanism.

For the NH_3 concentrations, most of the measured data are either well predicted or underpredicted, and only a few points are overpredicted.

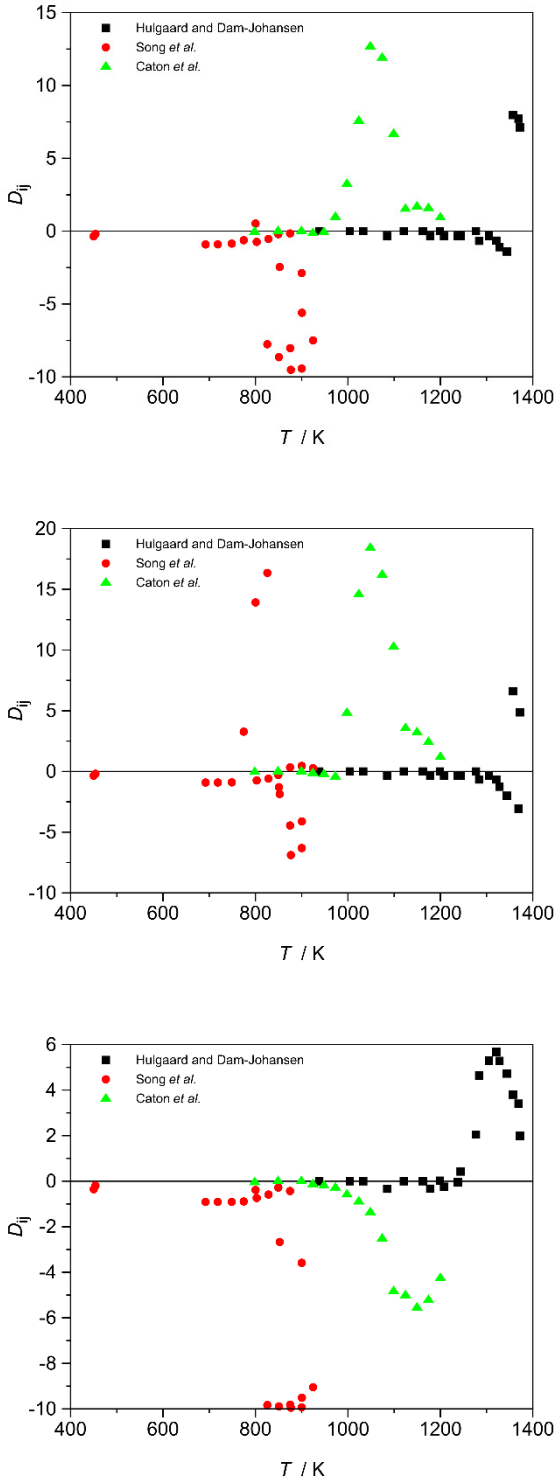

Fig. 10. Plot of the D_{ij} values versus temperature calculated by mechanisms Klippenstein-2011 (a), Glarborg-2018 (b) and Song-2019 (c) for the N_2O concentration measurements.

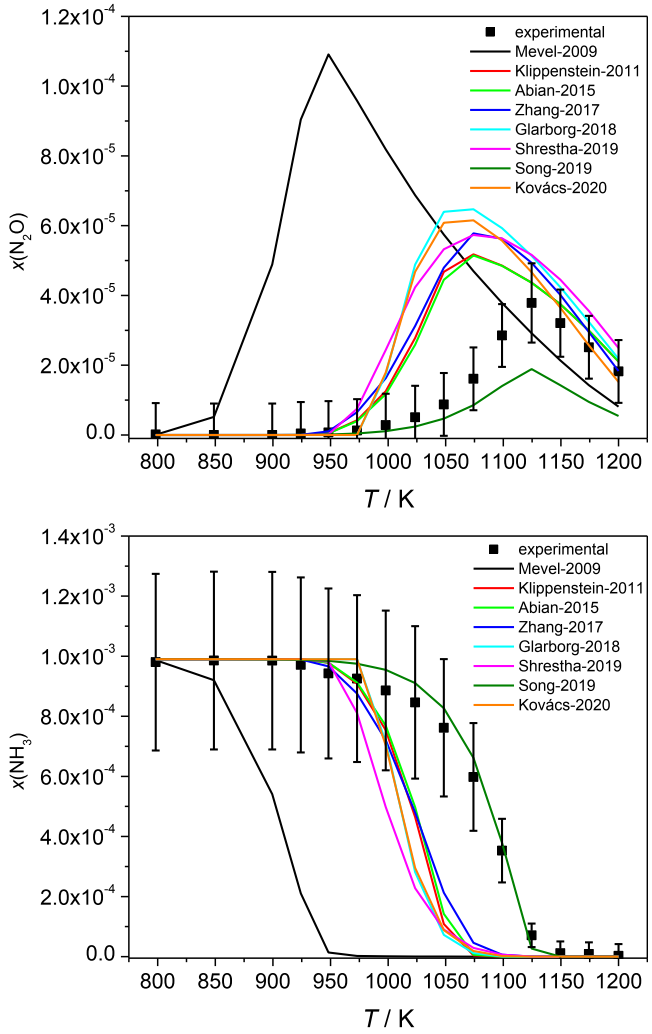

Fig. 11. N_2O and NH_3 concentration measurements of Caton et al. [36] (pressure 102 kPa, inlet mole fractions $x(NH_3)=0.00099$, $x(O_2)=0.150$, $x(N_2)=0.84901$) and the simulation results with all investigated mechanisms. The indicated error bars belong to 3σ. The simulation results are given with solid lines for each investigated mechanism.

Figure 11 presents the N_2O and NH_3 concentration – temperature plot for the reproduction of one experimental series of Caton et al. [36]. This figure can be used to interconnect the traditional "measurement points – error bars – simulation results given by lines" type visualization with the *E* and *D* values given in Tables 6 and 7, respectively and Figures 9 and 10. Figure 11 shows that the temperature location of the nitrous oxide concentration peak is predicted well by the Song-2019 mechanism, but it underpredicts the value of the maximum concentration. All other mechanisms overpredict the maximum concentration and the maximum appears at lower temperatures than the

experimental one. The temperature dependence of the ammonia concentration is predicted well by the Song-2019 mechanism. The other mechanisms predict the concentration decrese of NH_3 at much lower temperatures than the measured one.

8 Conclusions

Ammonia is a potentionally important fuel of the near future [1,2] because it is easy to handle and may be used for the efficient storage of electric energy generated by photovoltaic or wind turbine systems. This is the reason why many papers were published in the last two years on the chemical kinetics of NH_3 combustion. [1,3,4,22,23,30]

Experimental conditions and results of ignition delay time measurements in shock tubes and concentration measurements in flow reactors were collected from the literature and stored in ReSpecTh Kinetic Data Format version 2.2 data files. These files are available from the Respecth Information web site [27].

We expect that several new papers will appear in the coming years which will include the testing of new mechanisms for ammonia combustion. Using these RKD files and the accompanied codes available from the ReSpecTh web page [27], testing new mechanisms will be easier and faster. Also, a major part of our work was the assessment of measurement errors for each dataset based on the values reported in the original experimental papers and the scatter of the measurements. The obtained estimated errors are available in the Supplementary Material.

In this work, simulations were performed in parallel with simulation packages FlameMaster and OpenSmoke++, and the results were in very good agreement with each other. Eight recent reaction mechanisms for NOx chemistry were used in the comparison. Although only one of them was originally developed for the description of NH3 combustion, but in accordance with other authors [1,3,4] we found that combustion NOx mechanisms provide a good starting point for the development of dedicated reaction mechanisms for simulation of ammonia combustion.

Ignition delay times are well reproduced by five mechanism, the best ones are Glarborg-2018 and Shrestha-2018. Concentrations in flow reactors are reproduced much less well. There is no single reaction mechanism which can provide acceptable results for any of the species concentration. Several

mechanisms predicted systematic over- or underprediction of the experimental measurements. The agreement of the measured and simulated data and the systematic deviations are given for each dataset in the Supplementary Material.

During the preparation of the revised version of this article two important papers were published. Stagni et al. [3] reported a wide-range investigation of the oxidation mechanism of ammonia. New experimental data were obtained in a jet-stirred reactor and a flow reactor under lean conditions covering operating temperatures (500 K ≤ T ≤ 2000 K). Ammonia conversion and the formation of products and intermediates were analyzed. The modelling studies were based on the Song et al. [26] mechanism, but this mechanism was significantly updated by determining new rate parameters for several ractions using theoretical calculations. The updated reactions included the ammonia decomposition reaction and the reactions of HNO.

Dagaut [4] investigated the oxidation of NH_3 with and without added NO in the temperature range 1100 to 1450 K. The results were modelled using four published reaction mechanisms. A new mechanism was also suggested by updating the Dagaut et al. mechanism [49].

The results presented in this article show that the quantitative description of homogeneous ammonia combustion is still a challenge. The recently appeared publications [3,4] indicate the direction of extension of the present reseach. We plan to take into account these newly published data and also considering the new proposed mechanisms in the testing. Also, the comparisons will be extended to rapid compression machine measurements [50,51], jet stirred reactors [3,4,52,53], burning velocity mesuraments [54–59] and burner stabilized flames [60]. Another task for the future is linking the selection of the rate parameters of the key elementary reactions with the simulation results using sensitivity and rate-of-production analyses.

Acknowledgements. The authors acknowledge the financial support of the Hungarian National Research, Development and Innovation Office via NKFIH grants K116117 and PD120776. The authors are also grateful for the supportive comments of the partners in COST collaboration CM1404 (SmartCats).

References

[1] Kobayashi H, Hayakawa A, Kunkuma KD, Somarathne A, Okafor EC. Science and technology of ammonia combustion. Proc

Combust Inst **37** (2019) 109. https://doi.org/10.1016/j.proci.2018.09.029.
[2] Valera-Medina A, Xiao H, Owen-Jones M, David WIF, Bowen PJ. Ammonia for power. Prog Energy Combust Sci **69** (2018) 63. https://doi.org/10.1016/j.pecs.2018.07.001.
[3] Stagni A, Cavallotti C, Arunthanayothin S, Song Y, Herbinet O, Battin-Leclerc F, et al. An experimental, theoretical and kinetic-modeling study of the gas-phase oxidation of ammonia. React Chem Eng **5** (2020) 696. https://doi.org/10.1039/C9RE00429G.
[4] Dagaut P. On the oxidation of ammonia and mutual sensitization of the oxidation of NO and ammonia: experimental and kinetic modeling. Combust Sci Technol (2019) 1. https://doi.org/10.1080/00102202.2019.1678380.
[5] Olm C, Zsély IG, Pálvölgyi R, Varga T, Nagy T, Curran HJ, et al. Comparison of the performance of several recent hydrogen combustion mechanisms. Combust Flame **161** (2014) 2219. https://doi.org/10.1016/j.combustflame.2014.03.006.
[6] Olm C, Zsély IG, Varga T, Curran HJ, Turányi T. Comparison of the performance of several recent syngas combustion mechanisms. Combust Flame **162** (2015) 1793. https://doi.org/10.1016/j.combustflame.2014.12.001.
[7] Varga T, Nagy T, Olm C, Zsély IG, Pálvölgyi R, Valkó É, et al. Optimization of a hydrogen combustion mechanism using both direct and indirect measurements. Proc Combust Inst **35** (2015) 589. https://doi.org/10.1016/j.proci.2014.06.071.
[8] Varga T, Olm C, Nagy T, Zsély IG, Valkó É, Pálvölgyi R, et al. Development of a joint hydrogen and syngas combustion mechanism based on an optimization approach. Int J Chem Kinet **48** (2016). https://doi.org/10.1002/kin.21006.
[9] Olm C, Varga T, Valkó É, Curran HJ, Turányi T. Uncertainty quantification of a newly optimized methanol and formaldehyde combustion mechanism. Combust Flame **186** (2017) 45. https://doi.org/10.1016/j.combustflame.2017.07.029.
[10] Olm C, Varga T, Valkó É, Hartl S, Hasse C, Turányi T. Development of an ethanol

combustion mechanism based on a hierarchical optimization approach. Int J Chem Kinet **48** (2016) 423. https://doi.org/10.1002/kin.20998.

[11] Varga T, Zsély IG, Turányi T, Bentz T, Olzmann M. Kinetic analysis of ethyl iodide pyrolysis based on shock tube measurements. Int J Chem Kinet **46** (2014). https://doi.org/10.1002/kin.20829.

[12] Samu V, Varga T, Brezinsky K, Turányi T. Investigation of ethane pyrolysis and oxidation at high pressures using global optimization based on shock tube data. Proc Combust Inst **36** (2017) 691. https://doi.org/10.1016/j.proci.2016.05.039.

[13] Samu V, Varga T, Rahinov I, Cheskis S, Turányi T. Determination of rate parameters based on NH_2 concentration profiles measured in ammonia-doped methane–air flames. Fuel **212** (2018) 679. https://doi.org/10.1016/j.fuel.2017.10.019.

[14] Buczkó NA, Varga T, Zsély IG, Turányi T. Formation of NO in high-temperature $N_2/O_2/H_2O$ mixtures: re-evaluation of rate coefficients. Energy and Fuels **32** (2018) 10114. https://doi.org/10.1021/acs.energyfuels.8b00999.

[15] Kovács M, Papp M, Zsély IG, Turányi T. Determination of rate parameters of key N/H/O elementary reactions based on H_2/O_2/NOx combustion experiments. Fuel **264** (2020) 116720. https://doi.org/10.1016/j.fuel.2019.116720.

[16] Turányi T, Tomlin AS. Analysis of Kinetic Reaction Mechanisms. Springer; 2014. https://doi.org/10.1007/978-3-662-44562-4.

[17] Revel J, Boettner JC, Cathonnet M, Bachman JS. Derivation of a global chemical kinetic mechanism for methane ignition and combustion. J Chim Phys **91** (1994) 365.

[18] Mével R, Javoy S, Lafosse F, Chaumeix N, Dupre G, C-E P. Hydrogen-nitrous oxide delay times: shock tube experimental study and kinetic modelling. Proc Combust Inst **32** (2009) 359. https://doi.org/10.1016/j.proci.2008.06.171.

[19] Klippenstein SJ, Harding LB, Glarborg P, Miller JA. The role of NNH in NO formation and control. Combust Flame **158** (2011) 774. https://doi.org/10.1016/j.combustflame.2010.12.013.

[20] Miller JA, Glarborg P. Modeling the thermal De-NOx process: closing in on a final solution. Int J Chem Kinet **31** (1999) 757.
[21] Abian M, Alzueta MU, Glarborg P. Formation of NO from N_2/O_2 mixtures in a flow reactor: toward an accurate prediction of thermal NO. Int J Chem Kinet **47** (2015) 518. https://doi.org/10.1002/kin.20929.
[22] Zhang YJ, Mathieu O, Petersen EL, Bourque G, Curran HJ. Assessing the predictions of a NOx kinetic mechanism on recent hydrogen and syngas experimental data. Combust Flame **182** (2017) 122. https://doi.org/10.1016/j.combustflame.2017.03.019.
[23] Bugler J, Somers KP, Simmie JM, Güthe F, Curran HJ. Modeling nitrogen species as pollutants: thermochemical influences. J Phys Chem A **120** (2016) 7192. https://doi.org/10.1021/acs.jpca.6b05723.
[24] Glarborg P, Miller JA, Ruscic B, Klippenstein SJ. Modeling nitrogen chemistry in combustion. Prog Energy Combust Sci **67** (2018) 31. https://doi.org/https://doi.org/10.1016/j.pecs.2018.01.002.
[25] Shrestha KP, Seidel L, Zeuch T, Mauss F. Detailed kinetic mechanism for the oxidation of ammonia including the formation and reduction of nitrogen oxides. Energy & Fuels **32** (2018) 10202. https://doi.org/10.1021/acs.energyfuels.8b01056.
[26] Song Y, Marrodán L, Vin N, Herbinet O, Assaf E, Fittschen C, et al. The sensitizing effects of NO_2 and NO on methane low temperature oxidation in a jet stirred reactor. Proc Combust Inst **37** (2019) 667. https://doi.org/https://doi.org/10.1016/j.proci.2018.06.115.
[27] ReSpecTh webpage (2020). http://respecth.hu.
[28] PrIMe database (2011). http://www.primekinetics.org.
[29] Fujii N, Miyama H, Koshi M, Asaba T. Kinetics of ammonia oxidation in shock waves. Symp Combust **18** (1981) 873. https://doi.org/10.1016/S0082-0784(81)80091-4.
[30] Drummond LJ. High temperature oxidation of ammonia. Combust Sci Technol **5** (1972) 175. https://doi.org/10.1080/00102207208952518.
[31] Mathieu O, Petersen EL. Experimental and

modeling study on the high-temperature oxidation of ammonia and related NOx chemistry. Combust Flame **162** (2015) 554. https://doi.org/10.1016/j.combustflame.2014.08.022.

[32] Shu B, Vallabhuni SK, He X, Issayev G, Mosshammer K, Farooq A. Fernandes RX. A shock tube and modeling study on the autoignition properties of ammonia at intermediate temperatures. Proc Combust Inst **37** (2019) 205. https://doi.org/10.1016/j.proci.2018.07.074.

[33] Hulgaard T, Dam-Johansen K. Homogenous nitrous oxide formation and destruction under combustion conditions. AIChE J **39** (1993) 1342. https://doi.org/10.1002/aic.690390811.

[34] Wargadalam VJ, Löffler G, Winter F, Hofbauer H. Homogeneous formation of NO and N_2O from the oxidation of HCN and NH_3 at 600–1000 °C. Combust Flame **120** (2000) 465. https://doi.org/10.1016/S0010-2180(99)00107-8.

[35] Song Y, Hashemi H, Christensen JM, Zou C, Marshall P, Glarborg P. Ammonia oxidation at high pressure and intermediate temperatures. Fuel **181** (2016) 358. https://doi.org/10.1016/j.fuel.2016.04.100.

[36] Caton JA, Narney J K, Cariappa H C, Laster W R. The selective non-catalytic reduction of nitric oxide using ammonia at up to 15% oxygen. Can J Chem Eng **73** (1995) 345. https://doi.org/10.1002/cjce.5450730311.

[37] Dove JE, Wing SN. A shock-tube study of ammonia pyrolysis. Can J Chem **57** (1979) 670. https://doi.org/10.1139/v79-112.

[38] Pitsch H. FlameMaster v4.0 beta: a C++ computer program for 0D combustion and 1D laminar flame calculations (2016). https://www.itv.rwth-aachen.de/index.php?id=flamemaster&L=1.

[39] Cuoci A, Frassoldati A, Faravelli T, Ranzi E. OpenSMOKE++: an object-oriented framework for the numerical modeling of reactive systems with detailed kinetic mechanisms. Comput Phys Commun **192** (2015) 237. https://doi.org/10.1016/j.cpc.2015.02.014.

[40] OpenSmoke++ website (2020). https://www.opensmokepp.polimi.it/.

[41] NUI Galway Combustion Chemistry Centre. AramcoMech 2.0 (2016). http://www.nuigalway.ie/c3/aramco2/frontmatter.html.

[42] Nagy T. Minimal spline fit introducing root-mean-square fitting of data series with Akima splines (2020). http://respecth.hu.
[43] Alzueta MU, Røjel H, Kristensen PG, Glarborg P, Dam-Johansen K. Laboratory study of the $CO/NH_3/NO/O_2$ system: implications for hybrid reburn/SNCR strategies. Energy & Fuels **11** (1997) 716. https://doi.org/10.1021/ef960140n.
[44] Alzueta MU, Glarborg P, Dam-Johansen K. Low temperature interactions between hydrocarbons and nitric oxide: an experimental study. Combust Flame **109** (1997) 25. https://doi.org/10.1016/S0010-2180(96)00146-0.
[45] Espinosa-García J, Corchado JC. Recalibration of two earlier potential energy surfaces for the $CH_4 + H \rightarrow CH_3 + H_2$ reaction. application of variational transition-state theory and analysis of the kinetic isotope effects using rectilinear and curvilinear coordinates. J Phys Chem **100** (1996) 16561. https://doi.org/10.1021/jp961608q.
[46] Baulch DL, Bowman CT, Cobos CJ, Cox RA, Just T, Kerr JA, et al. Evaluated kinetic data for combustion modeling: Supplement II. J Phys Chem Ref Data **34** (2005) 757.
[47] Klaus P. Entwicklung Eines Detaillierten Reaktionsmechanismus Zur Modellierung Der Bildung von Stickoxiden in Flammenfronten. Ruprecht-Karls-Universität Heidelberg, Heidelberg, Germany, 1997.
[48] Sutherland JW, Patterson PM, Klemm RB. Flash photolysis-shock tube kinetic investigation of the reaction of oxygen(3P) atoms with ammonia. J Phys Chem **94** (1990) 2471. https://doi.org/10.1021/j100369a049.
[49] Dagaut P, Glarborg P, Alzueta M. The oxidation of hydrogen cyanide and related chemistry. Prog Energy Combust Sci **34** (2008) 1. https://doi.org/10.1016/j.pecs.2007.02.004.
[50] Pochet M, Dias V, Moreau B, Foucher F, Jeanmart H, Contino F. Experimental and numerical study, under LTC conditions, of ammonia ignition delay with and without hydrogen addition. Proc Combust Inst **37** (2019) 621. https://doi.org/10.1016/j.proci.2018.05.138.
[51] He X, Shu B, Nascimento D, Moshammer K, Costa M, Fernandes RX. Auto-ignition kinetics of ammonia and ammonia/hydrogen mixtures at intermediate temperatures and high

pressures. Combust Flame **206** (2019) 189. https://doi.org/10.1016/j.combustflame.2019.04.050.

[52] Dagaut P, Nicolle A. Experimental and kinetic modeling study of the effect of SO_2 on the reduction of NO by ammonia. Proc Combust Inst **30** (2005) 1211. https://doi.org/10.1016/j.proci.2004.07.029.

[53] Rota R, Antos D, Zanoelo EF, Carra S. Experimental study and kinetic modelling of nitric oxide reduction with ammonia. Combust Sci Technol **163** (2001) 25. https://doi.org/10.1080/00102200108955215 0.

[54] Ronney PD. Effect of chemistry and transport properties on near-limit flames at microgravity. Combust Sci Technol **59** (1988) 123. https://doi.org/10.1080/00102208808947092.

[55] Pfahl U., Ross M., Shepherd J., Pasamehmetoglu K., Unal C. Flammability limits, ignition energy, and flame speeds in H_2–CH_4–NH_3–N_2O–O_2–N_2 mixtures. Combust Flame **123** (2000) 140. https://doi.org/10.1016/S0010-2180(00)00152-8.

[56] Takizawa K, Takahashi A, Tokuhashi K, Kondo S, Sekiya A. Burning velocity measurements of nitrogen-containing compounds. J Hazard Mater **155** (2008) 144. https://doi.org/10.1016/j.jhazmat.2007.11.089.

[57] Hayakawa A, Goto T, Mimoto R, Arakawa Y, Kudo T, Kobayashi H. Laminar burning velocity and markstein length of ammonia/air premixed flames at various pressures. Fuel **159** (2015) 98. https://doi.org/10.1016/j.fuel.2015.06.070.

[58] Liu Q, Chen X, Huang J, Shen Y, Zhang Y, Liu Z. The characteristics of flame propagation in ammonia/oxygen mixtures. J Hazard Mater **363** (2019) 187. https://doi.org/10.1016/j.jhazmat.2018.09.073.

[59] Mei B, Zhang X, Ma S, Cui M, Guo H, Cao Z, et al. Experimental and kinetic modeling investigation on the laminar flame propagation of ammonia under oxygen enrichment and elevated pressure conditions. Combust Flame **210** (2019) 236. https://doi.org/10.1016/j.combustflame.2019.08.033.

[60] Maclean DI, Wagner HG. The structure of the reaction zones of ammonia-oxygen and hydrazine-decomposition flames. Symp Combust **11** (1967) 871. https://doi.org/10.1016/S0082-0784(67)80213-3.